Dosimetry of Rhenium-186-Labeled Monoclonal Antibodies: Methods, Prediction from Technetium-99m-Labeled Antibodies and Results of Phase I Trials

Hazel B. Breitz, Darrell R. Fisher, Paul L. Weiden, James S. Durham, Barbara A. Ratliff, Michael J. Bjorn, Paul L. Beaumier and Paul G. Abrams

Departments of Radiology and Medicine, Virginia Mason Medical Center, and NeoRx Corporation, Seattle, Washington; and Health Physics Department, Battelle Pacific Northwest Laboratories, Richland, Washington

Rhenium-186 is a beta-emitting radionuclide that has been studied for applications in radioimmunotherapy. Its 137 keV gamma photon is ideal for imaging the biodistribution of the immunoconjugates and for obtaining gamma camera data for estimation of dosimetry. Methods used for determining radiation absorbed dose are described. We have estimated absorbed dose to normal organs and tumors following administration of two different ^{186}Re-labeled immunoconjugates, intact NR-LU-10 antibody and the F(ab')$_2$ fragment of NR-CO-02. Tumor dose estimates in 46 patients varied over a wide range, 0.4–18.6 rads/mCi, but were similar in both studies. Accuracy of activity estimates in superficial tumors was confirmed by biopsy. Prediction of ^{186}Re dosimetry from a prior ^{99m}Tc imaging study using a tracer dose of antibody was attempted in the NR-CO-02 (Fab')$_2$ study. Although ^{99m}Tc was an accurate predictor of tumor localization and the mean predicted and observed radiation absorbed doses to normal organs compared favorably, ^{186}Re dosimetry could not be reliably predicted in individual patients. The methods described nevertheless provide adequate estimates of ^{186}Re dosimetry to tumor and normal organs.

J Nucl Med 1993; 34:908–917

Antibodies labeled with beta-emitting radionuclides are being evaluated to assess the feasibility of radioimmunotherapy (RIT). Methods to estimate radiation absorbed dose to the tumor target and to critical normal organs in patients from the associated low level radiation have evolved over the past decade (*1–7*). Many immunoconjugates have been studied including polyclonal antibodies (*1*), sheep (*3*) or murine monoclonal antibodies (*4,8–11*) or their fragments (*11,12*) and more recently, chimeric antibodies (*13,14*). Iodine-131 has been the most commonly used radiolabel. Data for dosimetry have been acquired by counting the gamma photons, estimating tissue retention times and applying Medical Internal Radiation Dose (MIRD) Committee methods with modifications for radiolabeled antibody kinetics (*1,15,16*). Dosimetry calculations for ^{90}Y-labeled antibodies have been more difficult because of the absence of gamma photons for counting (*6*). Although ^{111}In-labeled antibodies have been used to predict ^{90}Y dosimetry, the reliability of this approach remains controversial (*17*).

Rhenium-186 is an attractive radionuclide for RIT because of its physical and chemical properties (*15,18*). It has a 3.7-day half-life and emits a beta particle which is suitable for therapy. This beta particle has a maximum energy of 1.07 MeV; 90% of its energy is absorbed within 1.8 mm of a point source (*19*). Rhenium-186 is also suitable for imaging since the 137 keV photons emitted are ideal for gamma camera imaging. Bremsstrahlung losses account for 1% of counts in tissue and do not influence count detection (*20*). Dosimetry estimates can therefore be made by quantitation of gamma camera data. The low abundance (9%) of the 137 keV photon and of the higher energy photons (0.05% > 600 keV photons) result in minimal cross irradiation of normal organs and minimal radiation exposure to medical personnel compared with ^{131}I.

The chemistry of rhenium and technetium is similar; both can be stably linked to antibodies using a preformed amide thiolate chelate method (*21,22*) and biodistribution of ^{99m}Tc-labeled and ^{186}Re-labeled antibody in the nude mouse/human xenograft system is similar (*21,22*). We investigated the feasibility of using ^{99m}Tc and ^{186}Re as a "matched pair" for confirmation of tumor localization and treatment of malignant disease in two phase I trials using two different antibodies and have previously reported our clinical experience (*11*). A ^{99m}Tc immunoconjugate was used to determine localization in tumor and to select patients for therapy. One study used the pancarcinoma antibody, NR-LU-10 (*23*); the other used the F(ab')$_2$ fragment of anti-CEA variant antibody NR-CO-02 (*24*). In the NR-LU-10 study, the Fab fragment of NR-LU-10 was labeled

Received Aug. 7, 1992; revision accepted Jan. 11, 1993.
For correspondence or reprints contact: Hazel B. Breitz, MD, Virginia Mason Medical Center, 1100 Ninth Ave., P.O. Box 900, C5-NM, Seattle, WA 98111.

with ^{99m}Tc for imaging, and the intact antibody was labeled with ^{186}Re for therapy. In the NR-CO-02 study, the F(ab')$_2$ fragment could be used for both imaging (^{99m}Tc-labeled) and therapy (^{186}Re-labeled) because its serum half-life was short enough to be compatible with ^{99m}Tc imaging. We postulated that use of a ^{99m}Tc-immunoconjugate might permit accurate determination of the optimal ^{186}Re activity to be administered for RIT. Therefore, we attempted to predict ^{186}Re dosimetry from the prior ^{99m}Tc study.

In this report, we describe our methods for quantitation of ^{186}Re activity and dose estimation and the results of the attempted dosimetry predictions. We also compare our results with those previously reported for ^{131}I-labeled murine antibody dosimetry (*1,8–10*).

METHODS

Patients with refractory carcinomas were studied if their tumors localized the ^{99m}Tc-immunoconjugate (*11*). In general, ^{186}Re-immunoconjugate was administered within 15 days of the imaging study (*11*). Tumor location and volume were determined by CT scan. Details of patient selection, antibody labeling using a preformed chelate and study design have been previously published (*11*).

Prediction of ^{186}Re dosimetry was undertaken in 24 patients who received ^{99m}Tc. Images were acquired immediately and at 3, 8 and 24 hr after the ^{99m}Tc-immunoconjugate and immediately and at 3, 20, 44, 68 and 140 hr following the ^{186}Re-immunoconjugate. Blood, urine and fecal specimens were obtained during the first week following the ^{186}Re administration (*11*). Tissue biopsies were obtained in four patients to determine the percent of the injected dose of antibody per gram (%ID/g) of tumor. The excised tissue samples were counted in a gamma counter (Minaxi Gamma) with a calibration standard of known activity.

In Vivo Quantitation of Activity. A GE 400AT Starcam II (General Electric, Milwaukee, WI) digital gamma camera was used to acquire and process all data. Images were acquired using a 15% window over the 137 keV photopeak of ^{186}Re. A medium-energy collimator was used to reduce the scatter contribution from the 0.05% abundance higher energy gamma photons (*25*). Quantitative planar imaging was performed to determine the activity in the source organs at each timepoint (*26–28*).

Simple phantom studies were performed to examine the attenuation of ^{186}Re. The transmission of counts from ^{99m}Tc and ^{186}Re in water was compared in a Jaszczack phantom (Data Spectrum, Chapel Hill, NC). The fraction of counts transmitted was essentially identical for ^{99m}Tc and ^{186}Re and was unchanged when either a low-energy, all-purpose or a medium-energy collimator was used. The comparison of transmitted counts using a medium energy collimator is shown in Table 1. For the conjugate view method, a flat flood source was placed beneath the imaging table and a 5 min image was acquired and stored on computer (*28*). Then a transmission image of the patient's chest and abdomen was obtained and regions of interest (ROIs) were drawn over the lungs, liver and tumor when appropriate to calculate an attenuation factor. In six patients who had attenuation factors derived from both a ^{99m}Tc and a ^{186}Re flood source, the results were similar. For example, the mean attenuation factor for the lungs was 1.92 ± 0.13 for ^{99m}Tc and 1.97 ± 0.18 for ^{186}Re. We subsequently used 10–15 mCi of ^{99m}Tc to obtain transmission data for attenuation factors.

TABLE 1
Comparison of Transmitted Counts Using a Medium Energy Collimator

Depth (cm)	Percent counts transmitted		Percent difference
	^{99m}Tc (190 μCi)	^{186}Re (1000 μCi)	
2.4	82.5	81.9	0.6
3.8	71.6	71.3	0.3
5.2	60.4	61.4	1.0
6.6	51.9	51.1	0.8
8.0	43.9	44.1	0.2
9.4	37.7	37.4	0.3
10.8	31.2	31.3	0.1
12.2	26.2	25.6	0.6
13.6	22.1	22.1	0
15.0	18.9	18.7	0.2
16.4	15.6	16.1	0.5
17.8	13.4	13.5	0.1
19.2	11.3	11.5	0.2
20.6	9.5	9.8	0.3

To estimate the attenuation from source organs which were seen on only one view, we used an attenuation factor based on depth. Depth of the source organs, i.e. kidneys and many tumors, was estimated by CT scan which measured from the center of the organ to the skin surface (*13*). We used conditions of broad beam geometry to represent the clinical situation in order to derive attenuation factors, rather than the linear attenuation coefficient for the 137 keV photon (*20*). We derived a curve comparing the fraction of counts transmitted from the source as a function of depth in water and used the inverse of this as the effective attenuation factor. This represented scatter as well as attenuation. The background subtracted counts from one view (*2*) were multiplied by this attenuation factor.

At each imaging session, the patient's anterior chest was first imaged for 1 million counts or 5 min, whichever was shorter. All other images were of equal duration. Anterior and posterior images of the head, chest, abdomen, pelvis and any other relevant views for tumor imaging were acquired. Whole body counts were obtained from a 6-min gamma camera whole body scan. The fraction of the administered activity remaining at each time point was determined from background subtracted counts. This method produced essentially identical results to those obtained using the patient as a point source and counting at a distance with a thyroid probe. A 250-ml tissue culture flask with approximately 10 mCi of ^{186}Re was counted at 25 cm for 1 min as a calibration standard for the camera following each imaging session. In a typical patient study, the camera sensitivity was 3.03 cpm/μCi.

The geometric mean of the anterior and posterior counts was obtained from selected ROIs to determine activity within the liver and lungs using the conjugate-view method for gamma camera imaging (*26–28*). To reduce the contribution of scatter from surrounding organs with high activity, we determined size of the organs in pixels using a ROI surrounding the whole organ and measured average counts per pixel in a smaller ROI, drawn to exclude as much scatter as possible from neighboring organs (*28*). For example, counts per pixel in the lungs were obtained from a region distant from the cardiac blood pool and liver. Liver counts per pixel were obtained from a ROI drawn when prominent kidney or large intestinal activity was present, but which included as much normal liver as possible. The identical ROI, which was at least 50% of the whole organ size, was used at each time point.

The average counts per pixel in the smaller ROI was then multiplied by the organ size in pixels to obtain total organ counts. Liver background subtraction was attempted using CT scans to estimate true background thickness but was time consuming and resulted in only a 2%–3% difference in cumulative activity. Therefore, we elected to estimate liver activity without background subtraction.

Rhenium-186 immunoconjugate metabolites were excreted into the intestinal tract obscuring the kidneys on the anterior images. Kidney counts were therefore obtained only from posterior ROI and background activity was subtracted using an adjacent semicircular region. Counts from the testes and thyroid were obtained from anterior images only (*2*). A ROI over both testes was drawn and background activity from a scrotal ROI subtracted. A background region was drawn below the thyroid gland to subtract underlying activity in the neck blood vessels.

To estimate tumor activity, we modified planar quantitation methods (*13,27,28*) by subtracting background activity. In general, tumors were seen on only one view and the attenuation factor was derived based on tumor depth. When tumors were visualized on opposing views, the conjugate-view method was used. Background activity was subtracted from a region of similar tissue density close to the tumor. The proportion of background activity subtracted was based on relative tumor to whole body thickness from the CT scan. Tumor mass was determined by summation of the areas of contiguous CT slices.

Absorbed Dose Estimates. Methods recommended by the MIRD Committee were used to estimate radiation absorbed doses (*29–32*). Both penetrating and nonpenetrating radiation were considered. Information regarding the type of radioactivity, energy of radiation and yield of the decay pathways for ^{186}Re were added to the MIRDOSE2 software (Internal Dose Information Center at Oak Ridge Institute for Science and Education, Oak Ridge, TN) to calculate S-factors to assess organ doses. Absorbed doses to the whole body and to normal organs were estimated using the standard MIRD male/female anthropomorphic models. Corrections were made for patient mass and for liver mass when liver metastases were present. Absorbed doses to tumor tissues were estimated using the same approach taken for normal organs (*1,15,16*). S-factors for tumors were estimated by comparison with normal organs of similar mass and position in the body.

To estimate cumulative activity, we expressed the measured activity in selected source organs as a percent of administered activity (%ID) at each time point. Time-activity curves for each source organ or the remainder tissues were integrated to determine organ residence times. Infinite time integrals were estimated from the observed long-term exponential portion of the time activity curves.

Whole body, liver and lungs demonstrate activity within minutes of infusion and residence times, T_R, were determined by:

$$T_R = A_0/\lambda e,$$

where A_0 is the fraction of administered activity in the source organs soon after injection and λe is the effective clearance time constant, 0.693/Te. For organs with a slower uptake (e.g., kidney and some tumors), clearance from the point of highest activity, t_1, was fit as above but a linear fit was applied to the initial uptake data. In this case:

$$T_R = \frac{(A_0 + A_1)}{2}(t_1 - t_0) + \frac{A_1}{\lambda e},$$

where A_1 is the fraction of injected activity at t_1. In organs that continued to exhibit uptake till the last time point (e.g., thyroid following NR-LU-10). A linear fit of all the data was performed and from the last time point onward, physical decay only was assumed.

Activity in red marrow was not directly assessed. Red marrow dose was estimated using serum clearance (*33*) by:

$$T_{R,RM} = T_{R,S} \times (1 - Ht) \times M_{RM} \times F,$$

where RM = red marrow, S = serum, Ht = hematocrit, M = mass and F = ratio of the specific activity in marrow to circulating blood. This approach assumes that marrow clearance is similar to blood clearance and that the specific activity of the radionuclide in marrow is 0.25 of the specific activity of blood (*33,34*).

Because gut activity on the images was prominent, absorbed dose to the gastrointestinal tract from ^{186}Re in the gut lumen was estimated. Dosimetry was derived from the gastrointestinal biokinetic model described in ICRP Publication 30 (*35,36*) and MIRDOSE2. Dosimetry was based on estimates of residence time for activity clearing the body through the intestinal tract. We used clearance times of one-half of those in the model because we administered cathartics to decrease transit time. Cumulative excretion in the feces was measured. MIRDOSE2 assumes that the dose to the intestine is the same at the tissue surface as throughout the wall and that it is equal to 50% of the equilibrium absorbed dose to the luminal contents. However, the average path length of the nonpenetrating component of ^{186}Re is such that most of the beta energy is unable to reach the entire thickness of the intestinal wall mucosa. We estimated the amount of energy emitted from ^{186}Re that is absorbed in the intestinal walls from a radioactive source within the intestine to be only about 10% of the equilibrium absorbed dose. Because MIRDOSE2 estimates the absorbed energy to be 50% of the equilibrium absorbed dose, the intestinal dose is overestimated by 80%. The nonpenetrating component of ^{186}Re accounts for 91% of the dose absorbed by the intestine. The fraction of the total dose to the intestine from activity within the intestine is 98%, whereas 2% represents contributions from activity in other organs. Therefore, MIRDOSE2 overestimates the dose to the intestine by the quantity:

$$D_o = 0.80 \times 0.91 \times 0.98 = 0.71,$$

where D_o = dose overestimate for nonpenetrating radiation.

In order to calculate the absorbed dose to the entire thickness of the intestinal tract from both penetrating and nonpenetrating components, the calculated dose from MIRDOSE2 was multiplied by $1 - D_o = 1 - 0.71 = 0.3$. This modification should result in absorbed dose estimates that correlate better with biological response than the standard MIRDOSE2 estimates.

To predict dosimetry for ^{186}Re therapy from ^{99m}Tc F(ab')$_2$ NR-CO-02, we first calculated the effective half-times in source organs from the ^{99m}Tc activity curves. Assuming the biodistribution of ^{99m}Tc and ^{186}Re-NR-CO-02 F(ab')$_2$ to be similar (*21,22*), we estimated the effective half-time for the ^{186}Re-immunoconjugate from $1/Te^{186}Re = 1/Tb^{99m}Tc + 1/Tp^{186}Re$ (where Tb = biological half-time, Te = effective half-time and Tp = physical half-life of the radioisotope). This calculated value for the effective half-time of ^{186}Re was used to predict the absorbed dose to normal organs from the ^{186}Re-NR-CO-02 F(ab')$_2$ antibody to be administered. Tumor dosimetry was difficult to estimate from the ^{99m}Tc study because the short half-life of ^{99m}Tc resulted in insufficient data points to measure clearance from tumors.

RESULTS

Normal Organ Biodistribution and Dosimetry

Rhenium-186-NR-LU-10 Antibody. The mean whole body, liver, lung and kidney biodistribution determined in 15 patients is shown in Figure 1A. The gamma camera data were decay corrected and are expressed as percent injected activity over time. Clearance half-times were as follows: whole body, 66 ± 18 (s.d.) hr; liver, 66 ± 14 hr; and lungs 36 ± 6 hr. As blood pool activity in the whole body, liver and lungs decreased, kidney and intestinal activity became relatively more prominent. Kidneys were the primary route of radiolabel excretion. Maximum antibody concentration in the kidneys occurred on the second day, with a mean peak uptake of 2.1% total in both kidneys, followed by slow clearance, 239 ± 150 hr half-time. Prominent activity was seen in the large intestine, particularly from 48 hr on. The mean cumulative activity in feces in 11 patients was 15% ± 6% (*11*). Thyroid activity was noted due to cross-reactivity of the antibody with thyroid follicular cells (*23*). The thyroid gland was visualized by 20 hr with highest uptake of approximately 0.3% of the injected antibody at 140 hr. Testicular uptake was noted in most male patients. Although variable, activity usually increased until the third day and then decreased with a clearance half-time of 108 ± 75 hr. The estimated mean absorbed doses and the dose range in normal organs in all patients are shown in Table 2. The total rads received at the maximum tolerated dose level (90 mCi/m^2) are also indicated. Dose estimates for normal liver were based on the five patients without hepatic tumors. In only one patient (#49) was bone marrow activity visualized, perhaps related to a previous myeloproliferative disorder. An alternative method was used to calculate marrow dose for this patient. A lumbar vertebra was considered as a source organ to estimate marrow clearance half-time and 30% of the initial serum concentration was assumed as an estimate of the initial marrow activity. This marrow dose estimate was 2.56 rads/mCi (total dose 374 rads), compared with 0.91 rads/mCi (total dose 99 rads) using the serum clearance method alone. The former method was probably more

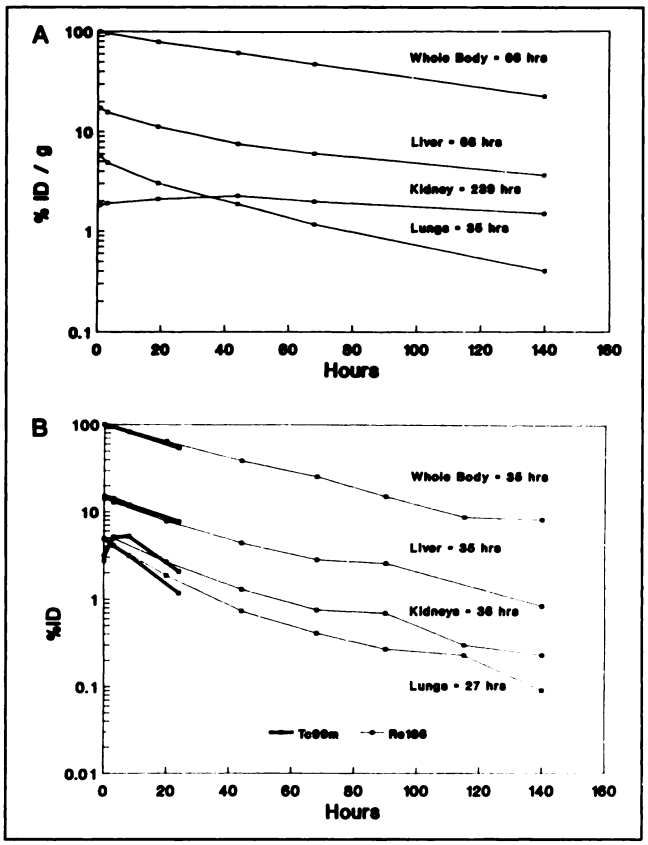

FIGURE 1. Biodistribution in normal organs determined by gamma camera imaging expressed as %ID. These curves are corrected for radionuclide decay. Biological clearance half-times are indicated for each organ. (A) ^{186}Re-NR-LU-10. (B) ^{99m}Tc (heavy line) and ^{186}Re (thin line) F(ab')$_2$ NR-CO-02.

TABLE 2
Rhenium-186-NR-LU-10 Normal Organ Dosimetry

	n	Absorbed dose (rads/mCi)			Total rads*
		Mean	s.d.	Range	
Whole body	15	0.59	0.18	0.41–0.97	100
Liver	5	2.93	0.45	2.25–3.65	475
Lung	9	1.39	0.39	0.89–2.09	225
Kidney	15	5.74	3.04	0.81–13.34	930
Marrow	15	1.01	0.31	0.69–1.55	165
Small intestine	11	0.16	0.04	0.11–0.20	30
ULI	11	0.54	0.18	0.40–0.76	90
LLI	11	1.38	0.50	0.98–1.97	225
Thyroid	13	2.45	1.73	0.49–6.04	280
Spleen	15	0.47	0.16	0.26–0.79	75
Ovary	6	0.59	0.16	0.34–0.79	95
Testis	9	1.30	1.24	0.20–4.45	210

*Mean total absorbed dose at maximum tolerated dose.
ULI = upper large intestine and LLI = lower large intestine.

TABLE 3
Rhenium-186-NR-CO-02 $F(ab')_2$ Normal Organ Dosimetry

	n	Absorbed dose (rads/mCi) Mean	s.d.	Range	Total rads*
Whole body	30	0.39	0.09	0.22–0.5	140
Liver	6	1.69	0.26	1.33–2.1	610
Lung	23	0.91	0.34	0.42–1.5	330
Kidney	30	3.49	1.50	0.87–6.5	1260
Marrow	30	0.73	0.18	0.37–1.12	260
Small intestine	19	0.13	0.03	0.06–0.18	47
ULI	20	0.48	0.15	0.09–0.83	170
LLI	20	1.24	0.41	0.14–2.19	450
Spleen	30	0.32	0.08	0.17–0.5	115
Ovary	11	0.34	0.13	0.23–0.5	120
Testis	9	0.66	0.79	0.12–1.9	240

*Mean total absorbed dose at highest dose level.
ULI = upper large intestine and LLI = lower large intestine.

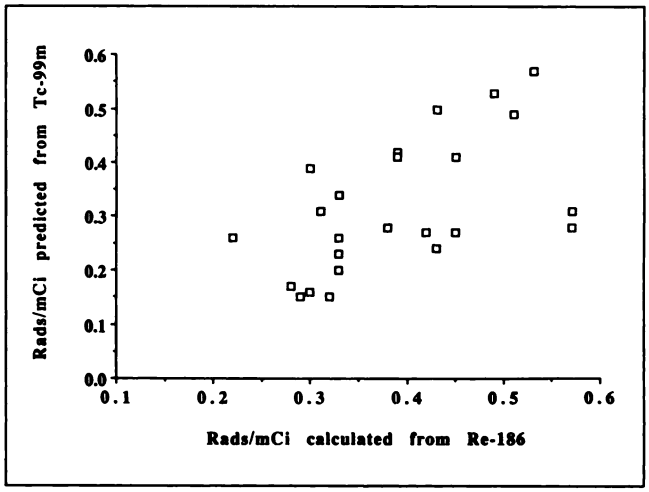

FIGURE 3. Correlation of radiation dose predicted and observed to whole body in 24 patients following NR-CO-02 $F(ab)_2'$. Dose predicted by ^{99m}Tc tracer per 1 mCi ^{186}Re is compared with dose estimated by ^{186}Re study.

accurate as the patient developed severe marrow toxicity at a relatively low administered dose (79 mCi/m^2). Severe marrow toxicity (grade III or IV platelet or white cell suppression) occurred in patients who received over 200 rads to their marrow.

Technetium-99m and Rhenium-186 NR-CO-02 $F(ab')_2$ Antibody. The mean biological clearance curves for whole body, liver, kidney and lung obtained from gamma camera imaging for both ^{99m}Tc and ^{186}Re in 24 patients are shown in Figure 1B. The mean biodistribution curves over the 24 hr of the ^{99m}Tc studies (heavy lines) can be superimposed on the initial 24 hr of the ^{186}Re studies (thin lines). The mean clearance half-time of the ^{186}Re-immunoconjugate for whole body was 35 ± 9 hr; liver 35 ± 1 hr; and lungs 27 ± 7 hr. Kidney activity peaked at 3–8 hr and then decreased with a 36 ± 14 hr half-time. Fecal excretion was similar to that following intact ^{186}Re antibody, i.e. 16% ± 7% (n = 20).

Table 3 shows results of the estimated radiation absorbed dose to various normal organs from ^{186}Re NR-CO-02 $F(ab')_2$ for 30 patients, including the mean, the range and total absorbed dose in rads at the maximum dose administered in patients with minimal prior therapy. In patients with extensive prior chemotherapy, severe marrow toxicity was observed at marrow doses above 160 rads (*11*).

Predictive Accuracy. The mean absorbed doses predicted from the ^{99m}Tc-NR-CO-02 $F(ab')_2$ tracer studies and the mean absorbed doses calculated from the ^{186}Re- NR-CO-02 $F(ab')_2$ therapy studies in 24 patients are presented graphically in Figure 2. While the mean values predicted and observed compare favorably, there was considerable individual patient variation particularly in determination of dose to the whole body. This appeared to be related to variability in clearance time. The whole body clearance time for the ^{186}Re fragment was 35 ± 9 hr while that of the ^{99m}Tc fragment was more variable, 33 ± 19 hr. Figure 3 shows a comparison of the predicted and calculated dose to the whole body. Paired t-tests indicated significant differences in predicted and actual dosimetry for whole body, marrow, lungs and kidney but no difference for liver. This variability was frequent and large enough to limit the predictive value for individual patients.

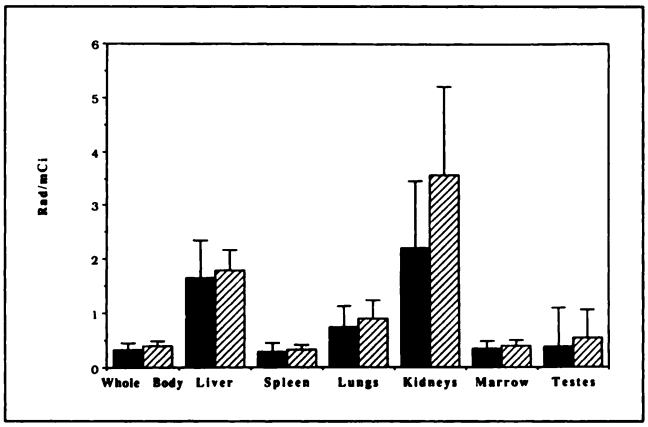

FIGURE 2. Mean absorbed doses in the whole body and various normal organs predicted from the ^{99m}Tc-$F(ab')_2$ NR-CO-02 study (solid bars) and subsequently calculated from the ^{186}Re-$F(ab')_2$ study (hatched bars). Number of observations varies from 24 for whole body to 6 for the liver.

Tumor Dosimetry

Rhenium-186-NR-LU-10 Antibody. The 3.7-day physical half-life of ^{186}Re allowed improved tumor visualization after the second day postadministration as blood pool activity decreased. The absorbed dose to tumor was estimated at the predominant site of disease if tumor volume could be assessed. Sites of metastases and details of the tumor do-

TABLE 4
Rhenium-186 NR-LU-10 Tumor Dosimetry

Patient no.	Tumor site	Absorbed Dose			^{186}Re uptake†		
		Liver + tumor (rads/mCi)	Lung + tumor (rads/mCi)	Tumor dose (rads/mCi)	%ID/g of tumor	Re^{186} uptake/g (μCi)	Tumor-to-whole body dose ratio
18	Liver	4.1		1.4			
36	Liver	5.4		nd			
37	Liver	3.7		8.3*–17.7	0.013	6.0	15.0
39	Liver	4.3		10.6*	0.021	20.2	14.1
40	Liver	3.9		14.1*	0.026	24.4	21.0
28	Lymph node			3.6			
42	Lung		2.2	2.7			
43	Lung		1.6	nd			
48	Liver	3.7		1.7–5.8*	0.011	16.1	12.4
46	Subcutaneous nodules* lungs		2.3	3.4*	0.006	10.7	6.5
49	Liver	3.8		4.5–11.0*	0.025	36.5	14.3
50	Lung		2.2	nd			
51	Liver	2.5		0.8			
54	Brain* lung liver	3.8	3.6	0.4*–10.1	0.017	30.6	0.4
55	Liver	2.8		5.1*	0.007	18.1	15.3
Mean		3.8	2.2	6.3	0.015	20.3	12.4
s.d.		0.8	0.6	4.8	0.008	10.1	6.3

A range of tumor dose estimates is indicated when multiple tumors were analyzed.
Data for eight tumors in last three columns is derived from tumors with an asterisk, i.e., those for which CT determined mass appeared accurate.
†Rhenium-186 uptake in tumor was determined at time of maximum uptake and is expressed as %ID/g and μCi ^{186}Re per g.

simetry are indicated in Table 4. When patients had multiple hepatic or pulmonary metastases, the absorbed dose to normal liver or lung tissue could not be estimated and the calculated dose to the organ included contributions from tumor masses. Because of specific uptake in the tumors, these "liver + tumor" and "lung + tumor" dose estimates were higher than the normal liver or lung doses. It was difficult to obtain accurate quantitation of activity in tumors within normal organs because of varying background activities (*37*) and because of the frequent difficulty in correlating CT tumor volumes with tumor ROI on planar images, particularly in lung lesions where fluid and atelectasis could not be distinguished from tumor. Activity was not high enough relative to background activity to draw accurate ROIs for all tumors. In patients with multiple small pulmonary nodules, tumor dose could not be estimated. Activity within the kidneys and intestine from immunoconjugate catabolites also caused difficulty in assessing antibody localization within abdominal masses and lymph nodes. Accepting these limitations, mean estimated absorbed dose for 20 tumors in 15 patients was 6.3 ± 4.8 rads/mCi.

Kinetics of immunoconjugates in tumors was examined using data from eight tumors which were separable from background activity and for which CT volume determinations appeared accurate (see Table 4 and Fig. 4). The mean percent of the injected activity per gram of tumor (%ID/g) at each time point was compared with the mean %ID/g whole body estimated from gamma camera data and the mean %ID/g serum for these patients (Fig. 4A). Tumor activity increased over the first 20 hr. The serum activity decreased with a half-time of approximately 25 hr and tumor activity was similar to serum activity at approximately 20 hr. The ratio of tumor-to-serum activity (Fig. 4B, hatched bars) increased with time to the end of data collection, and was 5:1 at 140 hr. Tumor-to-whole body activity ratios (Fig. 4B, solid bars) increased to a maximum of 17:1 at 68 hr.

Data from these tumors are detailed in the last three columns of Table 4. The variability of uptake and retention is indicated by the high standard deviations. From gamma camera estimates, the mean concentration was 0.015% ± 0.008% ID/g tumor at 20–40 hr and the mean tumor clearance half-time was 100 ± 84 hr. The mean tumor dose for these eight tumors was 6.1 ± 4.8 rads/mCi, and the tumor-to-whole body dose ratio ranged from 0.4–21.0 (mean 12.4).

Rhenium-186-NR-CO-02 F(ab')$_2$ Antibody. The ^{99m}Tc study was an accurate predictor of the ^{186}Re study in that all tumors visualized by ^{99m}Tc were seen with ^{186}Re (Fig. 5). Mean dose to liver with metastses was 2.1 ± 0.8 (n = 23) and lungs with metastases was 1.4 ± 0.9 (n = 6) which

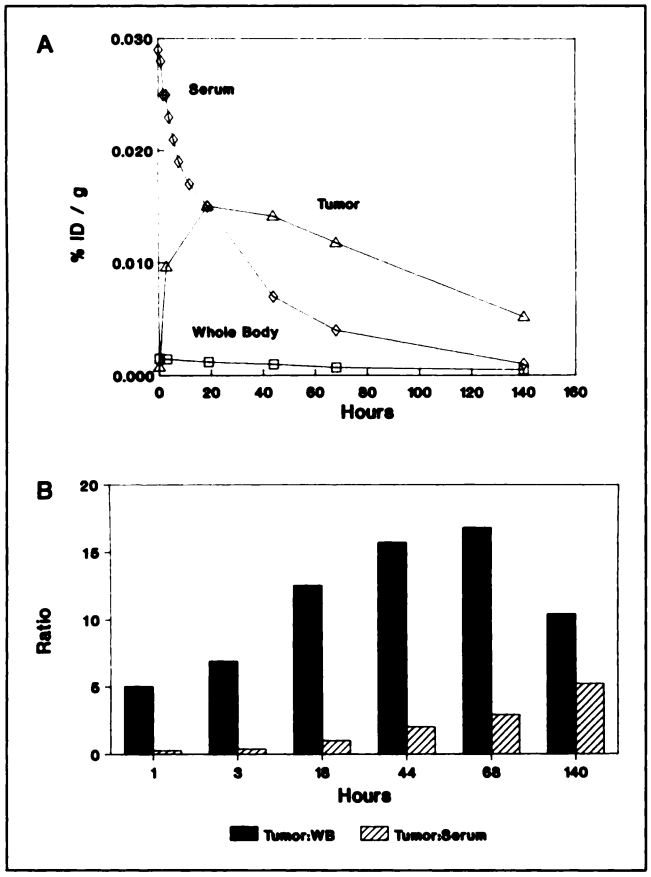

FIGURE 4. Tumor activity compared with serum and whole body activity expressed as %ID/g following ^{186}Re-NR-LU-10. (A) Curves show mean biodistribution in tumor, serum and whole body in eight patients. (B) Ratios of activity calculated from data shown in (A), i.e., tumor-to-whole body and tumor-to-serum at each time point.

was higher than the dose to the normal liver and lungs (Table 3), as with ^{186}Re-NR-LU-10. Tumor dosimetry was measurable in 41 tumors in 23 patients for which tumor volumes were estimated by CT scan. Individual estimates are not shown. Tumor absorbed doses ranged from 0.9 to 19 rad/mCi (mean ± s.d. = 4.0 ± 3.8 rads/mCi). From CT estimates of tumor mass, maximum uptake of ^{186}Re-NR-CO-02 antibody fragment occurred at 20 hr and ranged from 0.001 to 0.055%/g (mean 0.01 ± 0.01 %ID/g) and cleared with an average half-time of 57 ± 29 hr (Fig. 6A). The tumor-to-whole body dose ratio ranged from 0.9 to 54.6 (mean 10.2 ± 10.6). Tumor uptake was variable, even within individual patients. For example, in one patient the dose estimates ranged from 4.7 to 14.7 rads/mCi.

The mean curves of %ID/g for whole body, serum and tumor for ^{186}Re-NR-CO-02 are shown in Figure 6A. Mean tumor-to-serum ratios increased to 10:1 at 140 hr and the mean tumor-to-whole body ratio increased to 18:1 by 140 hr (Fig. 6B).

Correlation of Gamma Camera and In Vitro Dosimetry. Tumor tissue was excised in three patients from two lymph nodes and two subcutaneous nodules following ^{186}Re-NR-LU-10 so that the accuracy of the gamma camera estimation of %ID/g tumor could be verified by direct counting of a weighed tumor specimen. Similarly, two cervical lymph nodes were excised from one patient following ^{186}Re-NR-CO-02 F(ab')$_2$. The tumors were counted in vivo with the gamma camera prior to excision in three patients; in vivo gamma camera counts were too low in the third patient and the excised tissues were counted on the imaging table (ex vivo). The %ID/g ranged from 0.001% to 0.007% both in the gamma counter and from the gamma camera (mean 0.003%/g). The ratios of gamma camera to in vitro counter determination of %ID/g were 1.2, 1.1, 0.4, 0.7, 1.4 and 1.0 for the six specimens (mean 0.97) indicating good correlation and verifying the accuracy of the gamma camera quantitation for superficial tumors.

DISCUSSION

The physical properties of ^{186}Re resulted in good quality images for assessing immunoconjugate localization following administration of ^{186}Re-labeled murine monoclonal antibodies. This permitted the use of relatively simple procedures to quantitate activity from gamma camera images and derive dosimetry estimates. The resolution of the images was such that ROIs could be drawn on source organs without requiring administration of additional radionuclides to define organ boundaries (*17,27,40*) or blood-pool scans for background subtraction (*40*). We reduced the scatter contribution from high-energy gamma photons by using a medium energy collimator and a narrow spectrometric window at the 137 keV photopeak. Nevertheless, scatter from organs with high activity (kidneys and intestine) at later time points may have limited our ability to visualize uptake in some tumors and decreased the accuracy of quantitation. We compensated for this in normal organs by drawing smaller representative regions distant from areas of high activity and applied count per pixel information to organ size. Tissue sample data confirmed that estimates of activity from planar quantitation within superficial tumors (0.003% ID/g) were generally reliable.

The kidney absorbed dose estimates in the present studies are relatively high, possibly due to the slow clearance of metabolites from the kidneys. NR-LU-10 kidney doses may have been higher because of in vitro cross-reactivity of NR-LU-10 with collecting tubules (unpublished data) which probably accounts for the delayed clearance of NR-LU-10 from the kidneys (Fig. 1A) compared with NR-CO-02 (Fig. 1B). Severe myelosuppression was observed in three heavily pretreated NR-LU-10 patients (*11*); the whole body absorbed dose estimates were 128, 135 and 166 rads, and marrow doses were 297, 196 and 220 rads, respectively. Four heavily pretreated NR-CO-02 patients who developed severe marrow toxicity received 160, 163, 197 and 238 rads to bone marrow. Based on this experience, marrow doses above 160 rads are likely to result in

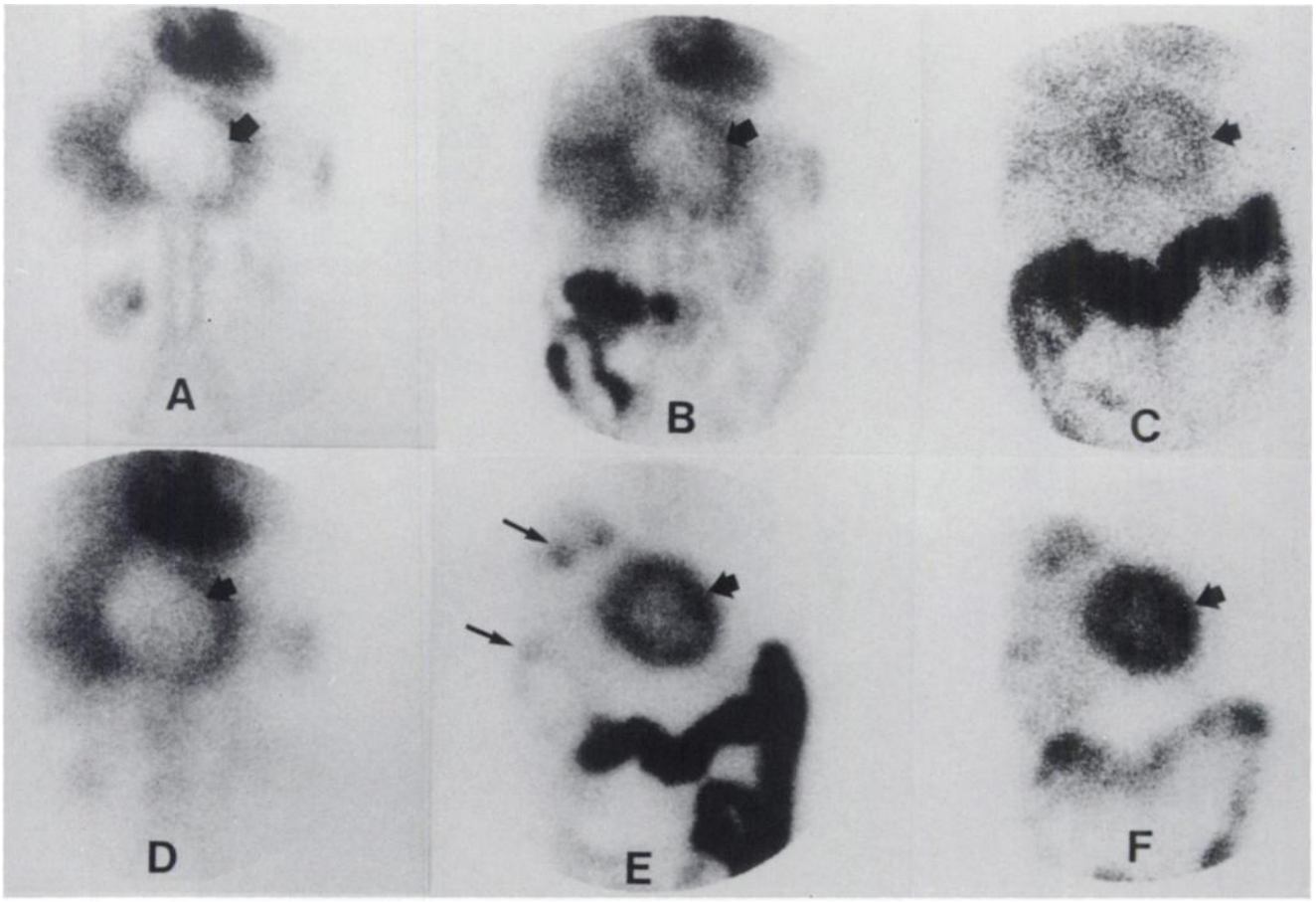

FIGURE 5. Anterior abdominal images following NR-CO-02. Top row: immediately (A), 8 hr (B) and 24 hr (C) after administration of ^{99m}Tc-NR-CO-02 F(ab')$_2$. Bottom row: immediately (D), 3 days (E) and 6 days (F) after administration of 236 mCi ^{186}Re-NR-CO-02 F(ab')$_2$. Thick arrows indicate a large hepatic metastasis from colon cancer; thinner arrows indicate several smaller metastases, best seen in images E and F. Note that metastatic lesions are initially photopenic, with specific uptake at later time points.

grade III or IV myelosuppression in patients who have been heavily pretreated.

The ^{99m}Tc-immunoconjugates were useful for selecting patients in that they both consistently predicted localization of the ^{186}Re-labeled antibody to tumor. One potential advantage of using the same antibody fragment and the same ligand for both imaging and therapy radionuclides was that ^{186}Re antibody dosimetry might be predictable from a prior ^{99m}Tc antibody study in each patient. In our patients in the NR-CO-02 F(ab')$_2$ study, the pharmacokinetics (*11*) and mean absorbed doses predicted from the ^{99m}Tc studies and calculated from the ^{186}Re studies compared favorably (Fig. 2), but there was considerable individual patient variation (Fig. 3) resulting in limited value of dosimetry predictions for any one patient. One possible explanation for the individual variation observed is that different antibody masses were administered in the two studies, i.e. approximately 18 mg of ^{99m}Tc-NR-CO-02 compared to 47 mg ^{186}Re-NR-CO-02 F(ab')$_2$. This included 10 mg of unlabeled antibody administered 10 min prior to each injection of labeled antibody. The lesser antibody mass of the ^{99m}Tc antibody fragment may have contributed to more variable clearance of the ^{99m}Tc-immunoconjugate. We were unable to correlate clearance half-times with either serum CEA or tumor burden. Thus, while the use of ^{99m}Tc and ^{186}Re-labeled immunoconjugates as a matched pair to predict tumor localization is feasible and practical, the use of this matched pair to predict dosimetry in individual patients requires additional study using doses identical in antibody mass.

We compared our clinical results of tumor to nontarget absorbed dose ratios with those predicted by Wessels and Rogus for ^{186}Re-labeled antibodies using theoretical modeling, prior to clinical data being available (*15*). These investigators predicted a tumor-to-whole body dose ratio of 8.5 with ^{186}Re for an intact antibody, similar to our observation of 10.7 (Table 4). The tumor-to-liver ratio determined in our studies (2:1) was lower than predicted, probably because of metabolism of the immunoconjugate in the liver resulting in higher than predicted liver doses. On the other hand, their predicted tumor-to-nontarget dose ratio of 5.7 for a F(ab')$_2$ fragment was lower than that determined in our study (10.2) because after 18 hr patient tumor-to-nontarget activity ratios were higher than predicted.

For these ^{186}Re-immunoconjugates the tumor-to-nontar-

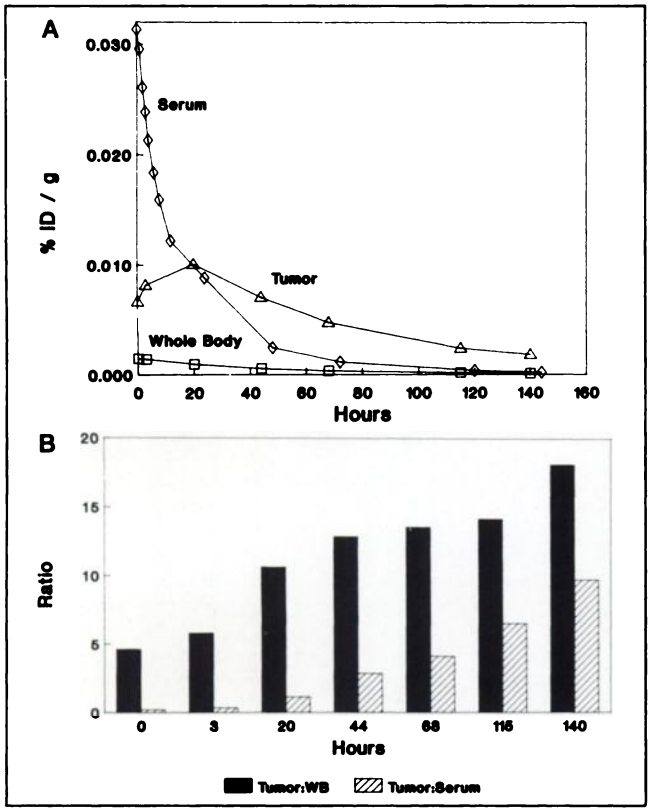

FIGURE 6. Tumor activity compared with serum and whole body activity expressed as %ID/g following ^{186}Re-F(ab')$_2$ NR-CO-02. (A) Curves show mean biodistribution in tumor, serum and whole body in 41 tumors in 23 patients. (B) Tumor-to-whole body and tumor-to-serum ratios.

get dose ratios were similar, i.e. tumor-to-liver = 2:1; tumor-to-lungs = 4:1; tumor-to-kidney = 1:1; tumor-to-marrow = 6:1; and tumor-to-whole body = 11:1. The peak uptake for both ^{186}Re-immunoconjugates in tumor as estimated from gamma camera data was typically 20 to 30 μCi/g, or approximately 0.01 %ID/g tumor. This resulted in a dose rate of 14–21 rads/hr.

Dosimetry results reported by various investigators for intravenously administered intact murine antibodies are summarized in Table 5. Iodine-131-labeled polyclonal antiferritin antibody (*1*) dose estimates in rads/mCi to normal organs and tumors are approximately twice that of ^{186}Re-NR-LU-10, although the tumor-to-whole body and tumor-to-liver dose ratios were similar. Doses to liver and kidneys were higher following ^{186}Re-NR-LU-10 than ^{131}I-labeled LL2 (*9*), MB1 and IF5 (*8*) probably due to metabolism and cross reactivity of the ^{186}Re-NR-LU-10 with renal tissue. Tumor dose estimates of four ^{131}I-monoclonal B-cell lymphoma antibodies are similar in rads/mCi to tumor dose estimates for ^{186}Re-immunoconjugates. Doses from ^{90}Y-labeled antibodies have not been estimated as rads/mCi administered. However, total absorbed dose to tumors appears similar to those from ^{131}I and ^{186}Re-labeled antibodies (*17*). Tumor doses for the ^{131}I and ^{186}Re-labeled monoclonal antibody studies were similar because the contribution of the penetrating and nonpenetrating radiation to a mass centrally located in the body yields a similar value of $\Sigma\Delta\phi_i$ for both ^{131}I and ^{186}Re (approximately 0.7 g-rad/mCi-hr). However, the dose from ^{186}Re is predominantly from the beta particle whereas the dose from ^{131}I is in substantial part from the high-energy gamma irradiation of ^{131}I which also results in up to 50% higher nontarget absorbed doses. Other advantages of ^{186}Re-immunoconjugates include the stability of the preformed chelate system, less marrow toxicity at comparable dose levels, simple procedures for quantitation of activity and the lower radiation exposure to medical personnel resulting in less need for patient isolation. We are continuing clinical trials with both intravenous and intra-peritoneal administration of ^{186}Re-labeled antibodies using these dosimetry methods.

ACKNOWLEDGMENTS

The authors thank T. Bernstein, PhD, and Stephen Cochoff of General Electric Medical systems for developing dosimetry software for the GE 400AT camera; J. Appelbaum, RN, and S. Wolf, RN, for clinical support during these trials; J-L Vanderheyden, PhD, D. Salk, MD, C. Seiler, CRA, M. Maurer, BS, T. Dodd, BS and A. Fritzberg, PhD of NeoRx Corp. for their support; W. Nelp, MD for initial assistance with in vivo quantitation; and B. Wessels, PhD for critical review of this paper.

TABLE 5
Dose Comparisons in rads/mCi

Radionuclide	Antibody	Tumor	Whole Body	Liver	Lung	Kidney	Reference
^{131}I	Polyclonal Antiferritin	16.6 ± 4.4	1.5 ± 0.3	6.2 ± 1.6			1
^{131}I	Monoclonal Lym-1	2-20					10
^{131}I	Monoclonal LL2	4.6 ± 1.9	0.6 ± 0.4	1.3 ± 0.8	1.3 ± 0.8	2.8 ± 1.6	9
^{131}I	Monoclonal MB1 IF5	4.6 ± 2.5	0.5 ± 0.3	1.9 ± 0.7	3.4 ± 1.9	1.9 ± 0.8	8
^{186}Re	Monoclonal NR-LU-10	6.3 ± 4.8	0.6 ± 0.2	2.9 ± 0.5	1.4 ± 0.4	5.7 ± 0.3	

REFERENCES

1. Leichner PK, Klein JL, Garrison JB, et al. Dosimetry of ^{131}I-labeled antiferritin in hepatoma: a model for radioimmunoglobulin dosimetry. *Int J Radiat Oncol Biol Phys* 1981;7:323–333.
2. DeNardo GL, Raventos A, Hines HH, et al. Requirements for a treatment planning system for radioimmunotherapy. *Int J Radiat Oncol Biol Phys* 1985;11:335–348.
3. Begent RHJ, Ledermann JA, Green AJ, et al. Antibody distribution and dosimetry in patients receiving radiolabeled antibody therapy for colorectal cancer. *Br J Cancer* 1989;60:406–412.
4. Klein JL, Nguyen TH, Laroque P, et al. Yttrium-90 and iodine-131 radioimmunoglobulin therapy of an experimental human hepatoma. *Cancer Res* 1989;49:6383–6389.
5. Eary JF, Press OW, Badger CC, et al. Imaging and treatment of B-cell lymphoma. *J Nucl Med* 1990;31:1257–1268.
6. Hantowich DJ, Mardirossian PD, Rose PG, et al. Intraperitoneal therapy of ovarian cancer with yttrium-90-labeled monoclonal antibodies: preliminary observations. *Antibody Immunoconj Radiopharm* 1991;4:359–371.
7. Siegel JA, Pawlyk DA, Lee RE, et al. Tumor, red marrow, and organ dosimetry for ^{131}I-labeled anticarcinoembryonic antigen monoclonal antibody. *Cancer Res* (Suppl 1) 1990;50:1039–1042.
8. Press OW, Eary JF, Badger CC, et al. Treatment of refractory non-Hodgkin's lymphoma with radiolabeled MB-1 (anti-CD37) antibody. *J Clin Oncol* 1989;7:1027–1038.
9. Goldenberg DM, Horowitz JA, Sharkey RM, et al. Targeting, dosimetry and radioimmunotherapy of B-cell lymphomas with iodine-131-labeled LL2 monoclonal antibody. *J Clin Oncol* 1991;9:548–564.
10. DeNardo SJ, DeNardo GL, O'Grady LF. Pilot studies of radioimmunotherapy of B-cell lymphoma and leukemia using ^{131}I Lym-1 monoclonal antibody. *Antibody Immunoconj Radiopharm* 1988;1:17–34.
11. Breitz HB, Weiden PW, Vanderheyden JL, et al. Clinical experience with rhenium-186-labeled monoclonal antibodies for radioimmunotherapy: results of phase I trials. *J Nucl Med* 1992;33:1099–1109.
12. Larson SM. Radioimmunology imaging and therapy. *Cancer* 1991;67:1253–1260.
13. Meredith RF, LoBuglio AF, Plott WE, et al. Pharmacokinetics, immune response and biodistribution of iodine-131-labeled chimeric mouse/human IgG1, k17-1A monoclonal antibody. *J Nucl Med* 1991;32:1162–1168.
14. Weiden P, Breitz H, Seiler C, et al. Rhenium-186-labeled chimeric antibody NR-LU-13: pharmacokinetics, biodistribution and immunogenicity. *Antibody Immunoconj Radiopharm* 1992;5:141.
15. Wessels B, Rogus RD. Radionuclide selection and model absorbed dose calculations for radiolabeled tumor associated antibodies. *Med Phys* 1984; 11:638–675.
16. Fisher DR, Badger CC, Breitz H, et al. Internal radiation dosimetry for clinical testing of radiolabeled monoclonal antibodies. *Antibody Immunoconj Radiopharm* 1991;4:655–664.
17. Leichner PK, Yang NC, Frenkel TL, et al. Dosimetry and treatment planning for ^{90}Y-labeled antiferritin in hepatoma. *Int J Radiation Oncology Biol Phys* 1987;14:1033–1042.
18. Volkert WA, Goeckeler GJ, Ketring AR. Therapeutic radionuclides: production and decay property considerations. *J Nucl Med* 1991;32:174–185.
19. Simpkin DJ, Mackie TR. EGS4 Monte Carlo determination of the beta dose kernal in water. *Med Phys* 1990;17:179–180.
20. Sorenson JA, Phelps ME. *Physics in nuclear medicine*. Orlando, FL: Grune and Stratton; 1980:174–186.
21. Fritzberg AR, Abrams PG, Beaumier PL, et al. Specific and stable labeling of antibodies with ^{99m}Tc with a diamide dithiolate chelating agent. *Proc Natl Acad Sci USA* 1988;25:4025–4029.
22. Vanderheyden JL, Rao TN, Kasina S, et al. Structural and biological equivalence of technetium and rhenium diamide dithiolate complexes: application of antibody labeling. In: Nicolini M, Bandoli G, Mazzi V, eds. *Technetium and rhenium in chemistry and nuclear medicine* New York: Raven Press 1990;623–630.
23. Varki NM, Reisfeld RA, Walker LE. Antigens associated with a human lung adenocarcinoma defined by monoclonal antibodies. *Cancer Res* 1984; 44:681–687.
24. Morgan AC, Woodhouse CS, Knost JA, et al. Monoclonal antibodies to human colorectal tumor-associated antigens: improved elicitation and subclass restriction. *Hybridoma* 1984;3:233–245.
25. Eary JF, Durack L, Williams D, et al. Considerations for imaging ^{188}Re and ^{186}Re isotopes. *Clin Nucl Med* 1990;15:911–916.
26. Thomas SR, Maxon HR, Keriakes JG. In vivo quantitation of lesion radioactivity using external counting methods. *Med Phys* 1976;3:253–255.
27. Hammond ND, Moldofsky PJ, Beardsley MR, et al. External imaging techniques for quantitation of distribution of ^{131}I F(ab')$_2$ fragments of monoclonal antibody in humans. *Med Phys* 1984;11:778–783.
28. Eary JF, Appelbaum FL, Durack L, et al. Preliminary validation of the opposing view method for quantitative gamma camera imaging. *Med Phys* 1989;16:382–387.
29. ICRU. Methods of assessment of absorbed dose in clinical use of radionuclides. In: *International Commission of Radiation Units and Measurements (ICRU) report* no. 32. Washington, DC: 1979.
30. NCRP. The experimental basis for absorbed dose calculations in medical uses of radionuclides. *National Council on Radiation Protection and Measurements (NRCP) report no. 83*. Bethesda, MD: 1985.
31. Lopvinger R, Budiayir, TF, Watson EEO. *MIRD primer for absorbed dose calculations.* New York: *Society of Nuclear Medicine*; 1988.
32. Snyder WS, Ford MR, Warner GG. Estimates of specific absorbed fractions for photon sources uniformly distributed in various organs of a heterogenous phantom. In: *MIRD pamphlet no. 5, revised.* New York: Society of Nuclear Medicine; 1978:5–67.
33. Siegel JA, Wessels BW, Watson EE, et al. Bone marrow dosimetry and toxicity for radioimmunotherapy. *Antibody Immunoconj Radiopharm* 1990; 3:213–233.
34. Buchegger F, Chalandon Y, Pèlegrin A, et al. Bone marrow dosimetry in rats using direct tissue counting after injection of radioiodinated intact monoclonal antibodies or F(ab')$_2$ fragments. *J Nucl Med* 1991;32:1414–1421.
35. ICRP. Limits for intakes of radionuclides by workers. In: *ICRP publication 30, part 1—annals of the ICRP*. Oxford, UK: Pergamon Press; 1979:30–34.
36. Eve IS. A review of the physiology of the gastrointestinal tract in relation to radiation dose from radioactive materials. *Health Phys* 1966;12:131–161.
37. Langmuir VK. Radioimmunotherapy: clinical results and dosimetric considerations. *Nucl Med Biol* 1992;19:213–225.
38. Welt S, Divgi CR, Real FX, et al. Quantitative analysis of antibody localization in human metastatic colon cancer: a phase I study of monoclonal antibody A33. *J Clin Oncol* 1990;8:1894–1906.